THE JOURNAL OF PHYSICAL CHEMISTRY C

Article

pubs.acs.org/JPCC

In Situ "Doping" Inverse Silica Opals with Size-Controllable Gold Nanoparticles for Refractive Index Sensing

Zhongyu Cai,[†,‡] Yan Jun Liu,[§] Xianmao Lu,*[,†] and Jinghua Teng*[,§]

[†]Department of Chemical and Biomolecular Engineering, National University of Singapore, 4 Engineering Drive 4, Singapore 117576

[‡]Department of Chemistry, University of Pittsburgh, Pittsburgh, Pennsylvania 15260, United States

[§]Institute of Materials Research and Engineering, Agency for Science, Technology and Research (A*STAR), 3 Research Link, Singapore 117602

Supporting Information

ABSTRACT: We report the fabrication of inverse SiO_2 opals "doped" with gold (i-Au-SiO_2-o) nanoparticles (NPs) via a co-self-assembly method combined with subsequent removal of polystyrene colloidal spheres by calcination. The resulting i-Au-SiO_2-o films demonstrate long-range ordering with uniform distribution of ligand-free Au NPs. The size of Au NPs can be tuned from 6 to 30 nm by varying the calcination temperature. The as-prepared i-Au-SiO_2-o films preserve both localized surface plasmon resonance (LSPR) and Bragg diffraction peaks simultaneously. Both LSPR and Bragg diffraction peaks are sensitive to the refractive index changes of the surrounding medium—an important feature for sensing applications. The method provides a facile and versatile way to fabricate high-quality Au NP "doped" photonic crystals for applications in sensing and others.

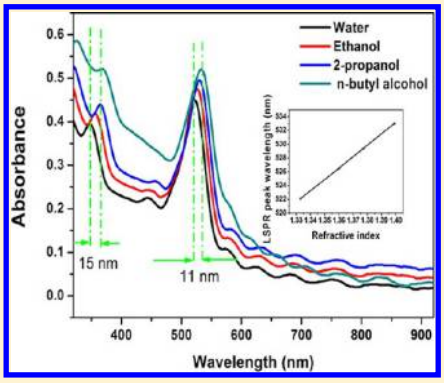

1. INTRODUCTION

Noble metallic nanoparticles (NPs) have attracted intense interests owing to their unique optical properties and have found extensive applications in areas, such as catalysis,[1] sensing,[2−5] and solar cells.[6,7] The root of their unique optical properties is the localized surface plasmon resonance (LSPR)—a phenomenon caused by the collective oscillation of surface electrons excited by incident light.[5,8] The LSPR of noble metal NPs is very sensitive to their geometrical and physical parameters, such as size, shape, composition, the distance between NPs, and the refractive index of the surrounding medium.[5,9,10] Another vastly studied optical property of nanostructured systems is the diffraction of light when a periodic modulation of the dielectric constant is achieved in the length scale of several hundreds of nanometers. Such systems are commonly termed as photonic crystals (PhCs), which has emerged as one kind of new optical material for various applications in photonics, water treatment, solar cells, and so on.[11−14] The hybridization of PhCs and noble metallic NPs can lead to structures with both LSPR and a photonic band gap (PBG) simultaneously,[15−17] opening up a whole range of possibilities for many applications, such as tunable photonic devices, biolabeling, and sensing.[18−20]

One common example of the hybridization of PhCs and noble metallic NPs is to immobilize as-synthesized Au NPs to a PhC. Gu et al. reported a dipping method to immobilize Au NPs on the surface of a prefabricated three-dimensional (3D) ordered SiO_2 opal film[15] and observed both LSPR of the NPs and the stop band of the PhC structures. Comparing with opal structures, inverse opals with both resonance peaks and diffraction peaks are especially desirable because they combine the advantages of high surface area with the accessible diffusion pathways associated with periodic macroporous structures.[21−23] Nevertheless, such a kind of structure has rarely been reported. This can be attributed to two major reasons: (1) the uniform distribution of noble metal NPs is very hard to control, and (2) the metal-dielectric inverse opals are not robust enough to support the framework due to various defects.[24] Few efforts have been made to overcome these impediments. A gold NP infiltrated polystyrene (PS) inverse opal was fabricated via a multistep approach, and both LSPR properties of Au NPs and photonic features of the PhCs were demonstrated.[16,25] However, many local disorders and defects exist in such a kind of hybrid inverse opals, which affect their optical properties severely and subsequent applications. Even worse, such a PS inverse opal structure is not robust enough to maintain the framework. In addition, the presence of capping molecules on the as-synthesized Au NP surface is highly undesirable for sensing and biolabeling applications since it results in damping and broadening of the plasmon band.[1,26] Therefore, Au "doped" silica (SiO_2) inverse opals were fabricated using silica-coated Au NPs as infiltration materials.[21,27] However, the quality of the resultant Au-infiltrated SiO_2 inverse opals was too poor to preserve both LSPR and PBG

Received: March 10, 2013
Revised: April 7, 2013
Published: April 12, 2013

Scheme 1. Fabrication of i-Au-SiO_2-o Films

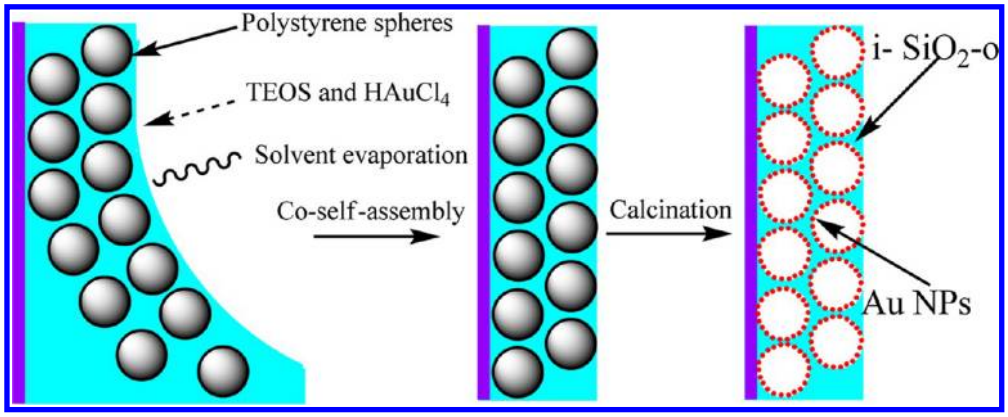

properties simultaneously. The cracks in the resultant films may cause the aggregation of Au NPs and consequently result in the plasmon coupling between particles in the proximity. In addition, these methods involve multistep fabrication (≥5 steps),[28] and they are very time- (4−5 d) and chemical-consuming. Thus, it remains challenging to achieve high-quality hybrids with both LSPR peaks and PBG peaks, which may give more accurate dual optical signatures.

Here,we report a facile coassembly method to fabricate high-quality Au NP "doped" inverse SiO_2 opal (i-Au-SiO_2-o) films over a large area. The Au NPs are uniformly distributed on the wall of the inverse SiO_2 opal (i-SiO_2-o) films. The effects of heat treatment temperature on Au NPs' size and optical properties of the i-Au-SiO_2-o films at different incident angles and ambient refractive index (RI) were investigated.

2. EXPERIMENTAL SECTION

Materials. All chemicals, including styrene (99%, Aldrich), potassium persulfate (99%, Aldrich), sulfuric acid (98%, Merck), hydrogen peroxide (35%, Scharlau Chemie S.A.), TEOS (98%, Aldrich), and hydrochloric acid (37%, Sigma-Aldrich), were used as received. $HAuCl_4 \cdot 3H_2O$ (49%, Aldrich) were used to prepare 0.02 M $HAuCl_4$ solution. Microscope cover glasses (22 mm × 22 mm × 0.3 mm, Deckgläser) were used as substrates for the fabrication of crack-free i-Au-SiO_2-o film. The glass substrates were treated in a piranha solution (3:1 v/v 98% H_2SO_4/35% H_2O_2) at 60 °C for 2 h before usage (*Caution!* Piranha solution and ethanol present potential health and/or fire hazards. Appropriate precautions should be observed at all times.)

Preparation of i-Au-SiO_2-o Film. The fabrication of i-Au-SiO_2-o film was conducted in two sequential steps: (a) co-self-assembly of PS colloidal crystals (CCs) with TEOS and $HAuCl_4$ and (b) calcination of the samples to remove PS (see Scheme 1). The fresh TEOS solution consisted of a 1:4:4 ratio by volume of TEOS, ethanol, and 0.02 M $HAuCl_4$, respectively, stirred at room temperature for 1 h prior to use. For a typical process, 243.2 μL of a 5.14 vol % PS (277 nm in diameter) colloidal suspension (cleaned by centrifugation at 8000 rpm at least three times) and 80 μL of hydrolyzed TEOS solution were sequentially added to 10 mL of deionized H_2O, and the mixture was sonicated for 5 min. The glass substrates were then vertically suspended in the vial containing the colloid/TEOS suspension. The solvent was evaporated slowly over a period of 24 h in an oven at 65 °C without disruption to allow the deposition of a thin film onto the suspended substrate. Afterward, the films were first calcined in air at 200 °C (0.5 °C/min) for 2 h to form Au NPs with a certain size, and finally at 450 °C (2 °C/min) for another 2 h, to completely remove the PS spheres and partially sinter the SiO_2 frame structure. It should be noted that the first calcination temperature can be varied from 110 to 280 °C to produce different sizes of Au NP infiltrated i-Au-SiO_2-o films.

Characterization. Scanning electron microscope (SEM) images of the PS CCs and i-Au-SiO_2-o were recorded using a JEOL JSM-6700F field emission SEM (FESEM). A field emission transmission electron microscope (FETEM, JEOL JEM-2100F) was employed to analyze the structure of the 3D macroporous i-Au-SiO_2-o films. Optical absorption spectra of the samples were measured with a Jasco V-530 UV−Vis spectrophotometer using unpolarized light. The absorption was measured at different angles, starting from normal incidence to 75° by increasing the angle in steps of 5°.

3. RESULTS AND DISCUSSION

Typical SEM images of PS/SiO_2 hybrid CCs and i-Au-SiO_2-o films are shown in Figure 1. Figure 1a demonstrates that highly ordered PS/SiO_2 colloidal crystal film was fabricated without cracks over a large domain using the coassembly method. Monodispersed PS spheres (277 nm in diameter) were assembled in a large domain (>500 × 500 μm^2) with long-range ordering (Figure S1 in the Supporting Information). The fast Fourier transformation (FFT) in Figure S1 (Supporting Information) indicates the high crystalline quality of the resultant CCs. By partially sintering the PS/SiO_2 colloidal crystal films at high temperature, their inverse structures were obtained (Figure 1b−f). A top view of the inverse opal reveals that 3D well-ordered macroporous structures were interconnected and exhibited a narrow pore size distribution (<0.6%) (Figure 1b). This highly ordered macroporous structure extended over a large area (>100 × 100 μm^2) without cracks (Figure 1c). This crack-free structural feature is very important since cracks may lead to aggregation of Au NPs and consequently result in a change of plasmon resonance and coupling among particles in the proximity, causing a shift of the resonant peak wavelength.[29] Crack-free i-Au-SiO_2-o films with different pore sizes can be fabricated by using PS beads of different sizes. Figure 1d shows an i-Au-SiO_2-o film fabricated with 428 nm PS colloidal spheres. In this case, a well-ordered structure with periodic macropores was achieved, indicating the effectiveness of the coassembly method. Panels e and f in Figure 1 are the cross-sectional images of i-Au-SiO_2-o film

dx.doi.org/10.1021/jp4024298 | J. Phys. Chem. C 2013, 117, 9440−9445

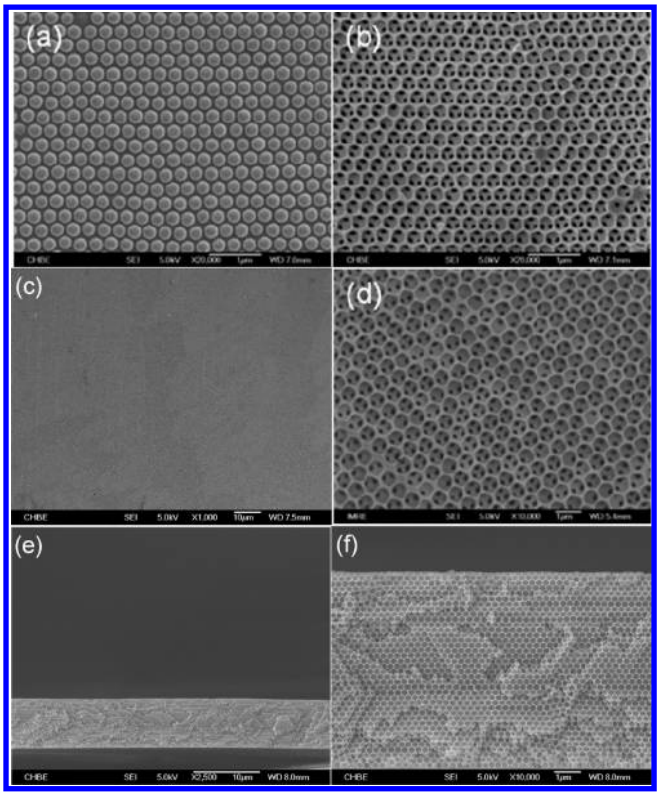

Figure 1. SEM images of the samples: (a–d) Top views of the PS/SiO_2 colloidal crystal film (277 nm), i-Au-SiO_2-o film (277 nm), i-Au-SiO_2-o film (277 nm) at low magnification, and i-Au-SiO_2-o film (428 nm) at high magnification, respectively. (e, f) Cross-sectional views of i-Au-SiO_2-o film (277 nm) at low and high magnifications, respectively.

fabricated with 277 nm PS colloidal spheres at low and high magnifications, respectively. Long-range ordering and a uniform thickness of ~8 μm of the film can be observed.

TEM measurements were carried out to characterize the Au NPs inside the i-Au-SiO_2-o films when calcinating the samples at 200 °C first. At low magnification (Figure 2a), a 3D periodically ordered i-SiO_2-o matrix can be observed with tiny dark dots (Au NPs) on the wall. A large amount of Au NPs were found uniformly distributed on the walls of the i-SiO_2-o film (Figure 2b). This cannot be achieved by conventional methods based on chemisorption, which generally results in uneven distribution or aggregation of Au NPs.[21,25,28] A higher magnification image (Figure 2c) shows that the Au NPs are single crystalline with an average diameter of 6 nm. Figure 2d shows a clear crystalline structure of a single Au NP with the size of ~6 nm when calcinating the samples at 200 °C first.

In addition to the even distribution of Au NPs on the wall of i-Au-SiO_2-o films, it is also found that the size of Au NPs can be tuned via varying the calcination temperature. When calcined at 200 °C (Figure 2c,d), the average size of Au NPs was ~6 nm. Highly ordered i-Au-SiO_2-o films can also be fabricated in a relatively large domain at the sintering temperature of 240 °C. Figure S2a (Supporting Information) shows the Au NPs with an average diameter of 15.6 nm when calcinating the samples at 240 °C first. Figure S2c (Supporting Information) shows an individual Au NP with a clear crystal structure fabricated at the sintering temperature of 240 °C. From the TEM analysis, the individual Au nanocrystal has a lattice constant of 2.36 Å, corresponding to {111} plane of a Au nanocrystal (Figure S2c,

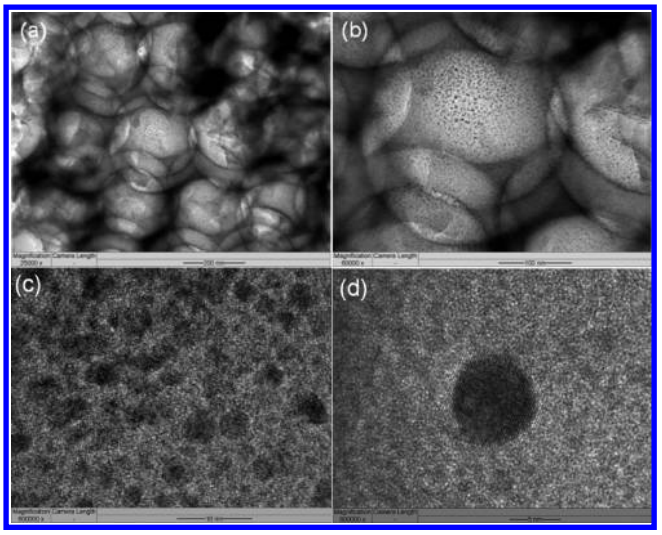

Figure 2. TEM images of i-Au-SiO_2-o samples. (a, b) Low- and high-magnification images of i-Au-SiO_2-o (277 nm) films, respectively. (c) Au NPs distributed on the walls of the i-Au-SiO_2-o film with an average diameter of ~6 nm. (d) Au NPs at high magnification show a diameter of ~6 nm.

Supporting Information). When sintering the samples first at 280 °C, the size of Au NPs further increases to ~30 nm on average with a relatively uniform size, as shown in Figure S2d (Supporting Information). These results showed that the size of the Au NPs can be effectively tuned by the sintering temperature. The LSPR properties of the i-Au-SiO_2-o films can be consequently controlled since the plasmonic properties of Au NPs are sensititve to their sizes.[1,9] In conventional methods, however, the size of Au NPs can only be tuned during the synthesis process, and subsequent chemisorption is needed.[21,25,28] The chemisorption usually leads to uneven distribution or aggregation of Au NPs on the wall of the i-Au-SiO_2-o films. Moreover, the chemisorption of molecules onto nanoparticles has been demonstrated to alter the electronic properties of Au NPs and consequently their extinction spectrum.[30] Further increasing the sintering temperatures, for example, to 300 °C, will cause the Au NPs to coalesce, resulting in a film with bulk Au properties (Figure S3, Supporting Information).

Despite the effectiveness of this method to fabricate high-quality i-Au-SiO_2-o films, to date, the underlying mechanism remains elusive to us. We believe that $HAuCl_4$ plays a vital role in the formation of high-quality i-Au-SiO_2-o films apart from acting as a source of Au NPs. While TEOS itself dissolves well in ethanol, its hydrolyzed form is hydrophilic and is, therefore, found inside the water-rich emulsion droplets.[31] Under the catalysis of $HAuCl_4$, the TEOS sol will form interconnected networks, which may provide sites for the relaxation of capillary forces generated during the processes of self-assembly and drying stage and thus avoid the formation of cracks in the resultant film.[32,33] In addition, controlled solvent release during the polycondensation reaction can also occur at the interfaces between the polymerizing sol–gel solution and the assembling PS colloidal spheres, and is channeled through the interconnected porous network to evaporate at the surface.[31,34]

Compared to conventional methods in fabricating Au NP infiltrated inverse opal structures,[21,25,28] our method is advantageous in the following aspects. First, high-quality samples can be fabricated in a controllable way. As shown in

dx.doi.org/10.1021/jp4024298 | J. Phys. Chem. C 2013, 117, 9440–9445

the SEM and TEM images, crack-free i-Au-SiO_2-o films can be fabricated in a relatively large area (~500 × 500 μm^2) without overlayers and the Au NPs can be uniformly distributed on the walls of the films. Moreover, the size of Au NPs can be tuned via calcination temperature. This approach provides a way to tune the response of the structure for applications, for example, sensors, with maximum sensitivity.[9] Second, our approach is facile, cost-effective, and robust. In our approach, the Au NPs with tunable sizes can be simultaneously in situ "doped" into i-SiO_2-o film during the process of formation of 3D highly ordered i-Au-SiO_2-o films. The present co-self-assembly and subsequent calcination step make our method straightforward. Conventional methods for the fabrication of Au NP "doped" opals or their inverse opals, however, often involve multiple steps, for example, synthesis of Au NPs, followed with chemisorptions of Au NPs on amine-functionalized opals or inverse opals. Amine-functionalized SiO_2 colloidal spheres are difficult to assemble into highly ordered CCs.[25] In addition, the modification of opals with amine groups (>12 h) and fabrication of inverse opals are very time-consuming (~4−5 d). Our method avoids the steps of synthesis of Au NPs, colloidal crystal modification, and removal of the excess regent. Thus, the present method is very facile. Finally, the Au NPs fabricated by this method are ligand-free, which is advantageous over those conventional ones since chemisorption of thiols to the Au NPs results in damping and broadening of the plasmon band.[1,26]

Au NPs are known to generate LSPR in the visible range, whereas PS CCs would have PBG characteristics. Figure S4a (Supporting Information) shows a typical UV−vis-NIR absorbance spectrum of the Au NP "doped" PS colloidal crystal film, where two characteristic peaks can be clearly observed. The absorption peak at 521 nm originates from the LSPR of individual Au NPs, whereas the other absorption peak at 612 nm arises from the pseudo stop band of the PS colloidal crystal template in a face-centered cubic (fcc) lattice. This is supported by both the SEM images shown in Figure 1a and the UV−vis-NIR absorbance spectrum of PS CCs (277 nm) in Figure S4b (Supporting Information) with a diffraction peak at 615 nm.

The diffraction peaks of PhCs depend on the incident angles and the effective refractive index of the surround media, whereas the LSPR peak position strongly depends on the size and shape of the particles as well as the dielectric properties of the surrounding media.[10,26,35,36] Here, we studied the effects of incident angles and refractive indices (RI) of surrounding media on the absorption spectra of the i-Au-SiO_2-o films. Figure 3 shows the evolution of absorption spectra of the i-Au-SiO_2-o films at different incident angles. At the incident angle of 90°, two clear absorption peaks at 357 and 522 nm can be observed, which are attributed to the Bragg diffraction and LSPR effects, respectively. This can be confirmed from the absorption spectrum of a SiO_2 inverse opal without Au NP "doping" but fabricated from the same size of PS spheres, which shows only one absorption peak at 357 nm (Figure S5, Supporting Information). With the decrease of the incident angle from 90° to 75°, the Bragg diffraction clearly shows blue shifted peaks with a slightly increased peak intensity. The observed blue shifts can be attributed to the change in diffraction according to the Bragg equation.[14,37] In contrast, the LSPR peak position does not change with incident angles. This is expected since the Au NPs are uniformly distributed on the wall of the i-SiO_2-o films and should generate incident-angle-

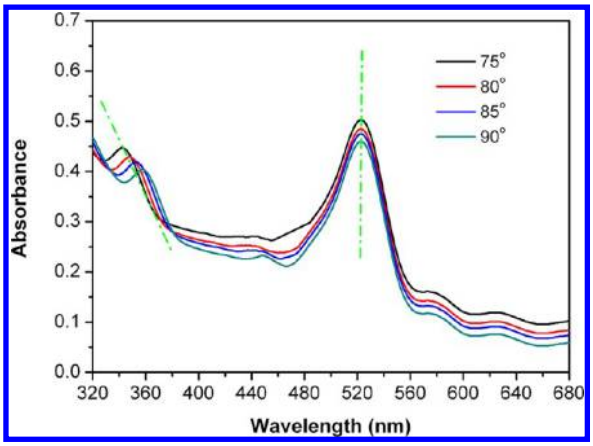

Figure 3. Absorption spectra of the i-Au-SiO_2-o films with 277 nm pores doped with 16 nm Au NPs at different incident angles.

independent resonance according to Mie's theory.[38,39] Therefore, the separation of LSPR and PBG peaks of the i-Au-SiO_2-o films can be effectively controlled by varying the incident angle.

Both LSPR and PBG are sensitive to the RI of the surrounding medium. In this study, deionized water, ethanol, 2-propanol, and *n*-butyl alcohol were used as dielectric media to investigate the sensitivity of the structure to external media change. The absorption spectra of the i-Au-SiO_2-o films infiltrated with different liquids in the interstices were measured and are shown in Figure 4. With the increase of the RI from

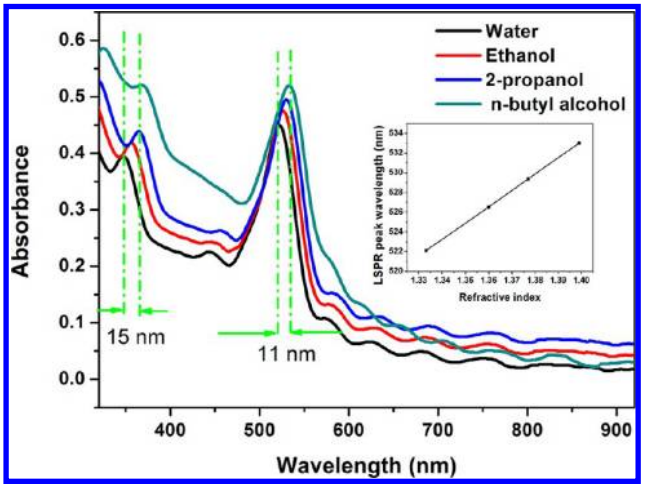

Figure 4. Absorption spectra of i-Au-SiO_2-o films with 277 nm pores infiltrated with media of varying RIs as follows: (a) water (n = 1.333), (b) ethanol (n = 1.360), (c) 2-propanol (n = 1.377), and (d) *n*-butyl alcohol (n = 1.399). The inset is the plot of the LSPR peak wavelength as a function of the refractive index of the surrounding medium.

1.333 to 1.399, the Bragg diffraction peak red shifts from 350 to 365 nm, which can be attributed to the change in effective RI of the i-Au-SiO_2-o.[40] The LSPR peaks red shift from 522 to 533 nm as a linear function of the surrounding RI, giving a sensitivity of 166 nm/RI unit (Figure 4, inset) that is higher than the value reported in the literature.[41−43] This can be attributed to the relatively uniform distribution of the Au NPs on the wall surfaces of the inverse opals. The Au NP "doped" SiO_2 inverse opal structure gives double indicators for RI change at both microscale from LSPR and macroscale from PBG, providing more confirmative information for sensing. In

dx.doi.org/10.1021/jp4024298 | J. Phys. Chem. C 2013, 117, 9440−9445

addition to a red shift of its resonance wavelength, an increase in the absorbance intensity can be observed as well, which is in accord with Mie theory.[44]

4. CONCLUSION

We have developed a facile method to fabricate high-quality i-Au-SiO_2-o films free of cracks over a large area (>100 × 100 μm^2). The in situ "doping" of Au NPs with tunable sizes and the formation of a three-dimensional ordered macroporous structure occur in the same step. The Au NPs are uniformly distributed on the wall of i-SiO_2-o films. By controlling the sintering temperature, the size of the Au NPs can be effectively tuned from 6 to 30 nm. The i-Au-SiO_2-o films show both LSPR of individual Au NPs and PBG of i-SiO_2-o films, which serve as two indicators for sensing of change in RI of the surrounding medium.

■ ASSOCIATED CONTENT

Supporting Information

Absorbance spectrum of PS CCs infiltrated Au NPs, PS CCs (277 nm), and SiO_2 inverse opals (277 nm), and FETEM image of i-Au-SiO_2-o fabricated film fabricated via calcination at 240, 280, and 300 °C. This material is available free of charge via the Internet at http://pubs.acs.org.

■ AUTHOR INFORMATION

Corresponding Author

*Telephone: (65) 6516 1071 (X.L.), (65) 6874 8590 (J.T.). Fax: (65) 6779 1936 (X.L.), (65) 6872 0785 (J.T.). E-mail: chelxm@nus.edu.sg (X.L.), jh-teng@imre.a-star.edu.sg (J.T.).

Notes

The authors declare no competing financial interest.

■ ACKNOWLEDGMENTS

Z.C. acknowledges a graduate scholarship from the National University of Singapore. This work was supported by the Ministry of Education of Singapore under Grant No. R279-000-298-112 and the Agency for Science, Technology and Research (A*STAR) under Grant Nos. 0921540099 and 0921540098.

■ REFERENCES

(1) Link, S.; El-Sayed, M. A. Spectral Properties and Relaxation Dynamics of Surface Plasmon Electronic Oscillations in Gold and Silver Nanodots and Nanorods. *J. Phys. Chem. B* **1999**, *103*, 8410−8426.

(2) Haes, A. J.; Chang, L.; Klein, W. L.; Van Duyne, R. P. Detection of a Biomarker for Alzheimer's Disease from Synthetic and Clinical Samples Using a Nanoscale Optical Biosensor. *J. Am. Chem. Soc.* **2005**, *127*, 2264−2271.

(3) Mayer, K. M.; Hafner, J. H. Localized Surface Plasmon Resonance Sensors. *Chem. Rev.* **2011**, *111*, 3828−3857.

(4) Saha, K.; Agasti, S. S.; Kim, C.; Li, X.; Rotello, V. M. Gold Nanoparticles in Chemical and Biological Sensing. *Chem. Rev.* **2012**, *112*, 2739−2779.

(5) Willets, K. A.; Van Duyne, R. P. Localized Surface Plasmon Resonance Spectroscopy and Sensing. *Annu. Rev. Phys. Chem.* **2007**, *58*, 267−297.

(6) Pala, R. A.; White, J.; Barnard, E.; Liu, J.; Brongersma, M. L. Design of Plasmonic Thin-Film Solar Cells with Broadband Absorption Enhancements. *Adv. Mater.* **2009**, *21*, 3504−3509.

(7) Standridge, S. D.; Schatz, G. C.; Hupp, J. T. Toward Plasmonic Solar Cells: Protection of Silver Nanoparticles via Atomic Layer Deposition of TiO_2. *Langmuir* **2009**, *25*, 2596−2600.

(8) Barnes, W. L.; Dereux, A.; Ebbesen, T. W. Surface Plasmon Subwavelength Optics. *Nature* **2003**, *424*, 824−830.

(9) Nath, N.; Chilkoti, A. Label-Free Biosensing by Surface Plasmon Resonance of Nanoparticles on Glass: Optimization of Nanoparticle Size. *Anal. Chem.* **2004**, *76*, 5370−5378.

(10) Lu, X.; Rycenga, M.; Skrabalak, S. E.; Wiley, B.; Xia, Y. Chemical Synthesis of Novel Plasmonic Nanoparticles. *Annu. Rev. Phys. Chem.* **2009**, *60*, 167−192.

(11) Cai, Z.; Teng, J.; Xia, D.; Zhao, X. S. Self-Assembly of Crack-Free Silica Colloidal Crystals on Patterned Silicon Substrates. *J. Phys. Chem. C* **2011**, *115*, 9970−9976.

(12) Ge, J.; Yin, Y. Responsive Photonic Crystals. *Angew. Chem., Int. Ed.* **2011**, *50*, 1492−1522.

(13) Galisteo-López, J. F.; Ibisate, M.; Sapienza, R.; Froufe-Pérez, L. S.; Blanco, Á.; López, C. Self-Assembled Photonic Structures. *Adv. Mater.* **2011**, *23*, 30−69.

(14) Cai, Z.; Teng, J.; Xiong, Z.; Li, Y.; Li, Q.; Lu, X.; Zhao, X. S. Fabrication of TiO_2 Binary Inverse Opals without Overlayers via the Sandwich-Vacuum Infiltration of Precursor. *Langmuir* **2011**, *27*, 5157−5164.

(15) Gu, Z.-Z.; Horie, R.; Kubo, S.; Yamada, Y.; Fujishima, A.; Sato, O. Fabrication of a Metal-Coated Three-Dimensionally Ordered Macroporous Film and its Application as a Refractive Index Sensor. *Angew. Chem., Int. Ed.* **2002**, *41*, 1153−1156.

(16) Ding, S.; Qian, W.; Tan, Y.; Wang, Y. In-Situ Incorporation of Gold Nanoparticles of Desired Sizes into Three-Dimensional Macroporous Matrixes. *Langmuir* **2006**, *22*, 7105−7108.

(17) Yi, D. K.; Lee, J.-H.; Rogers, J. A.; Paik, U. Two-Dimensional Nanohybridization of Gold Nanorods and Polystyrene Colloids. *Appl. Phys. Lett.* **2009**, *94*, 084104−3.

(18) Kuai, S.-L.; Bader, G.; Ashrit, P. V. Tunable Electrochromic Photonic Crystals. *Appl. Phys. Lett.* **2005**, *86*, 221110−3.

(19) Fan, H.; Yang, K.; Boye, D. M.; Sigmon, T.; Malloy, K. J.; Xu, H.; López, G. P.; Brinker, C. J. Self-Assembly of Ordered, Robust, Three-Dimensional Gold Nanocrystal/Silica Arrays. *Science* **2004**, *304*, 567−571.

(20) García-Santamaría, F.; Salgueiriño-Maceira, V.; López, C.; Liz-Marzán, L. M. Synthetic Opals Based on Silica-Coated Gold Nanoparticles. *Langmuir* **2002**, *18*, 4519−4522.

(21) Wang, D.; Salgueiriño-Maceira, V.; Liz-Marzán, L. M.; Caruso, F. Gold−Silica Inverse Opals by Colloidal Crystal Templating. *Adv. Mater.* **2002**, *14*, 908−912.

(22) Kuncicky, D. M.; Prevo, B. G.; Velev, O. D. Controlled Assembly of SERS Substrates Templated by Colloidal Crystal Films. *J. Mater. Chem.* **2006**, *16*, 1207−1211.

(23) Tessier, P. M.; Velev, O. D.; Kalambur, A. T.; Rabolt, J. F.; Lenhoff, A. M.; Kaler, E. W. Assembly of Gold Nanostructured Films Templated by Colloidal Crystals and Use in Surface-Enhanced Raman Spectroscopy. *J. Am. Chem. Soc.* **2000**, *122*, 9554−9555.

(24) Jones, M. R.; Osberg, K. D.; Macfarlane, R. J.; Langille, M. R.; Mirkin, C. A. Templated Techniques for the Synthesis and Assembly of Plasmonic Nanostructures. *Chem. Rev.* **2011**, *111*, 3736−3827.

(25) Tan, Y.; Qian, W.; Ding, S.; Wang, Y. Gold-Nanoparticle-Infiltrated Polystyrene Inverse Opals: A Three-Dimensional Platform for Generating Combined Optical Properties. *Chem. Mater.* **2006**, *18*, 3385−3389.

(26) Mulvaney, P. Surface Plasmon Spectroscopy of Nanosized Metal Particles. *Langmuir* **1996**, *12*, 788−800.

(27) Wang, D.; Li, J.; Chan, C. T.; Salgueiriño-Maceira, V.; Liz-Marzán, L. M.; Romanov, S.; Caruso, F. Optical Properties of Nanoparticle-Based Metallodielectric Inverse Opals. *Small* **2005**, *1*, 122−130.

(28) Wang, J.; Ahl, S.; Li, Q.; Kreiter, M.; Neumann, T.; Burkert, K.; Knoll, W.; Jonas, U. Structural and Optical Characterization of 3D Binary Colloidal Crystal and Inverse Opal Films Prepared by Direct Co-Deposition. *J. Mater. Chem.* **2008**, *18*, 981−988.

(29) Su, K. H.; Wei, Q. H.; Zhang, X.; Mock, J. J.; Smith, D. R.; Schultz, S. Interparticle Coupling Effects on Plasmon Resonances of Nanogold Particles. *Nano Lett.* **2003**, *3*, 1087−1090.

(30) Kreibig, U.; Bour, G.; Hilger, A.; Gartz, M. Optical Properties of Cluster−Matter: Influences of Interfaces. *Phys. Status Solidi A* **1999**, *175*, 351−366.
(31) Cai, Z.; Liu, Y. J.; Teng, J.; Lu, X. Fabrication of Large Domain Crack-Free Colloidal Crystal Heterostructures with Superposition Bandgaps Using Hydrophobic Polystyrene Spheres. *ACS Appl. Mater. Interfaces* **2012**, *4*, 5562−5569.
(32) Cai, Z.; Teng, J.; Yan, Q.; Zhao, X. S. Solvent Effect on the Self-Assembly of Colloidal Microspheres via A Horizontal Deposition Method. *Colloids Surf., A* **2012**, *402*, 37−44.
(33) Cai, Z.; Teng, J.; Wan, Y.; Zhao, X. S. An Improved Convective Self-Assembly Method for the Fabrication of Binary Colloidal Crystals and Inverse Structures. *J. Colloid Interface Sci.* **2012**, *380*, 42−50.
(34) Cai, Z.; Liu, Y. J.; Leong, E. S. P.; Teng, J.; Lu, X. Highly Ordered and Gap Controllable Two-Dimensional Non-Close-Packed Colloidal Crystals and Plasmonic-Photonic Crystals with Enhanced Optical Transmission. *J. Mater. Chem.* **2012**, *22*, 24668−24675.
(35) Kelly, K. L.; Coronado, E.; Zhao, L. L.; Schatz, G. C. The Optical Properties of Metal Nanoparticles: The Influence of Size, Shape, and Dielectric Environment. *J. Phys. Chem. B* **2002**, *107*, 668−677.
(36) Grzelczak, M.; Perez-Juste, J.; Mulvaney, P.; Liz-Marzan, L. M. Shape Control in Gold Nanoparticle Synthesis. *Chem. Soc. Rev.* **2008**, *37*, 1783−1791.
(37) Schroden, R. C.; Al-Daous, M.; Blanford, C. F.; Stein, A. Optical Properties of Inverse Opal Photonic Crystals. *Chem. Mater.* **2002**, *14*, 3305−3315.
(38) Mie, G. Beiträge zur Optik trüber Medien, speziell kolloidaler Metallösungen. *Ann. Phys.* **1908**, *330*, 377−445.
(39) Averitt, R. D.; Sarkar, D.; Halas, N. J. Plasmon Resonance Shifts of Au-Coated Au_2S Nanoshells: Insight into Multicomponent Nanoparticle Growth. *Phys. Rev. Lett.* **1997**, *78*, 4217−4220.
(40) Liu, Y. J.; Cai, Z.; Leong, E. S. P.; Zhao, X. S.; Teng, J. H. Optically Switchable Photonic Crystals Based on Inverse Opals Partially Infiltrated by Photoresponsive Liquid Crystals. *J. Mater. Chem.* **2012**, *22*, 7609−7613.
(41) Nath, N.; Chilkoti, A. A Colorimetric Gold Nanoparticle Sensor To Interrogate Biomolecular Interactions in Real Time on a Surface. *Anal. Chem.* **2001**, *74*, 504−509.
(42) Zheng, Y. B.; Juluri, B. K.; Mao, X.; Walker, T. R.; Huang, T. J. Systematic Investigation of Localized Surface Plasmon Resonance of Long-Range Ordered Au Nanodisk Arrays. *J. Appl. Phys.* **2008**, *103*, 014308−9.
(43) Liu, Y. J.; Hao, Q.; Smalley, J. S. T.; Liou, J.; Khoo, I. C.; Huang, T. J. A Frequency-Addressed Plasmonic Switch Based on Dual-Frequency Liquid Crystals. *Appl. Phys. Lett.* **2010**, *97*, 091101.
(44) Templeton, A. C.; Pietron, J. J.; Murray, R. W.; Mulvaney, P. Solvent Refractive Index and Core Charge Influences on the Surface Plasmon Absorbance of Alkanethiolate Monolayer-Protected Gold Clusters. *J. Phys. Chem. B* **1999**, *104*, 564−570.